

1 **Supporting Information**

2 **Asymmetric Electrode Configurations Enhance Operating Power Density and Energy**

3 **Efficiency of the Aqueous, Electrode-decoupled Titanium-Cerium Redox Flow Battery**

4 *Jing Xie^a, Shrihari Sankarasubramanian^{b,c}, Vijay Ramani^{a,*}*

5 ^aDepartment of Energy, Environmental and Chemical Engineering, Washington University in St.
6 Louis, St. Louis, MO 63130, USA

7 ^bDepartment of Biomedical Engineering and Chemical Engineering, The University of Texas
8 at San Antonio, San Antonio, TX 78249, USA.

9 ^cDepartment of Mechanical, Aerospace and Industrial Engineering, The University of Texas
10 at San Antonio, San Antonio, TX 78249, USA.

11 *Corresponding author

12 Author e-mails: xiejing@wustl.edu (J. Xie); shrihari.sankarasubramanian@utsa.edu (S.
13 Sankarasubramanian); ramani@wustl.edu (V. Ramani)

14

15 **S1. Measurement of specific capacitance (C_s)**

16 Cyclic voltammetry (CV) was conducted with a three-electrode system utilizing carbon paper (CP)
17 or heat-treated carbon felt (HT CF) as the working electrode, respectively. The electrolyte was 0.1
18 M methanesulfonic acid (MSA) and potential range was 0.1 to 0.6 V vs. Ag/AgCl. For CP, the
19 scan rates were 40, 60, 80, and 100 mV/s; for HT CF, the scan rates were 1, 5, 10, and 20 mV/s,
20 as shown in Fig. S2. The double layer capacitance, C_{dl} , was calculated based on the following
21 equation:

22 $i = C_{dl} \times v$

23 where i is the current value at the middle point of scan range (0.35 V vs. Ag/AgCl), and v is scan
24 rate. The specific capacitance, C_s , was calculated by dividing C_{dl} with electrode surface area (1
25 cm^2). The results are listed in Table S2.

26 **S2. Measurement of polarization curves**

27 Symmetric cell with same electrode configuration (three layers of CP for Ce and one layer of HT
28 CF for Ti) and electrolyte composition (50% SOC) were used for measuring polarization curves.
29 The absolute value of current density was increased linearly from 0 to about 400 mA cm^{-2} with an
30 interval of 40 mA cm^{-2} . At each interval, the current density was held for 15 seconds, and the
31 average value of potential was taken as the one shown in polarization curve. To make sure that the
32 electrolyte remained 50% SOC, the electrolyte flown through the cell was drained into external
33 container instead of the original electrolyte reservoir. The polarization curves of charge and
34 discharge for Ti and Ce sides are depicted in Figure S3.

35

36

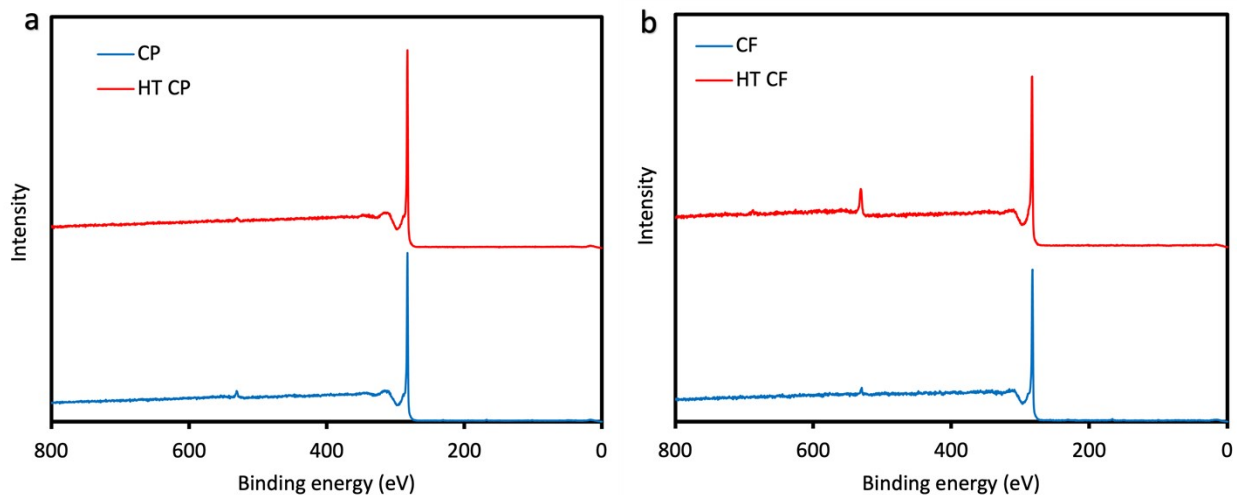
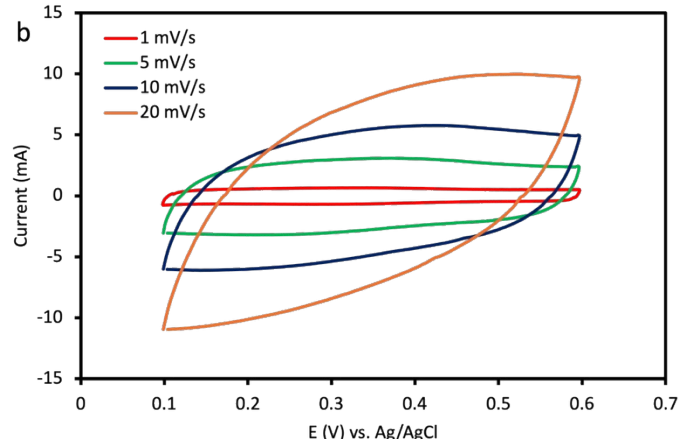
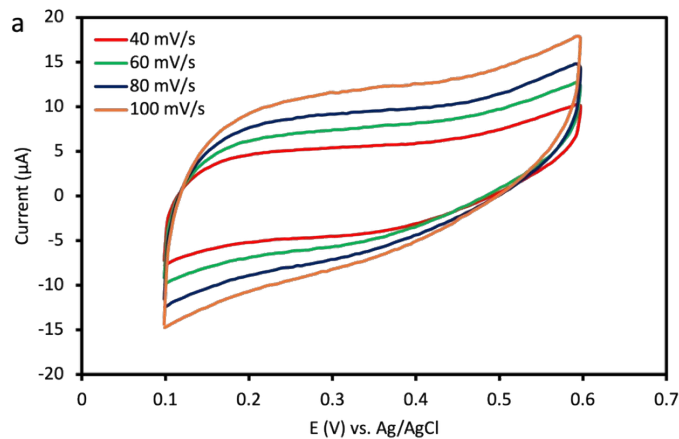


Figure S1. XPS survey of a) CP and HT CP, b) CF and HT CF.



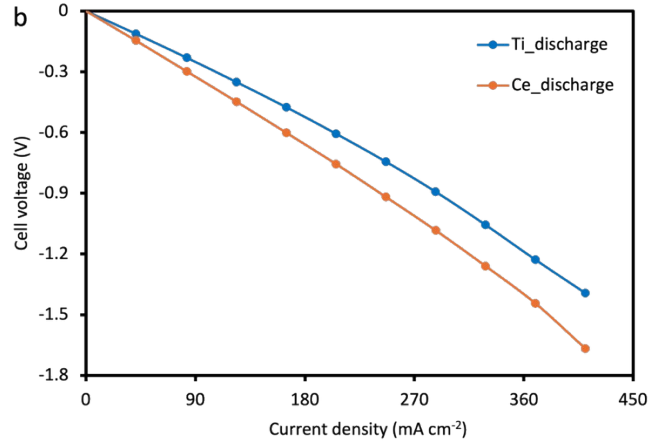
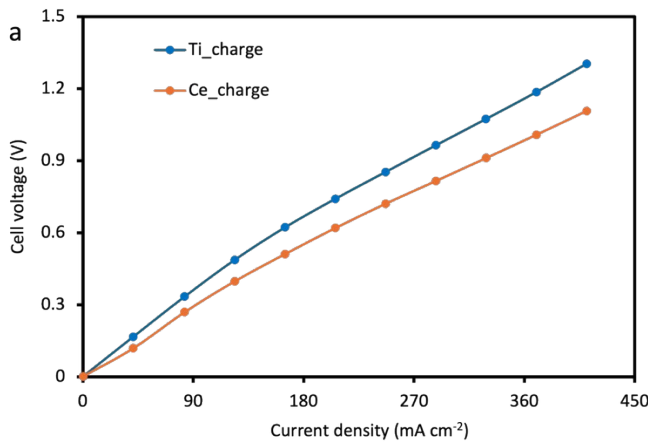
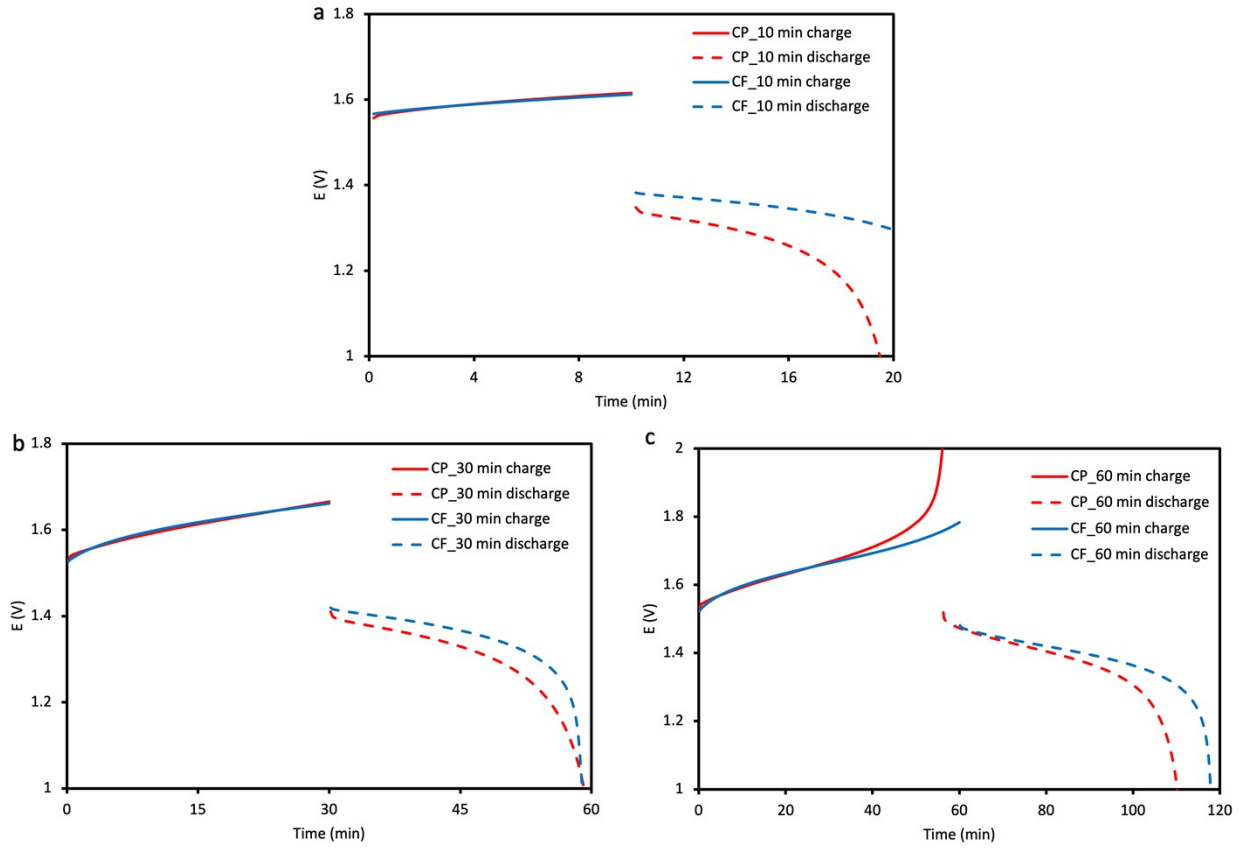


Figure S3. Polarization curves of a) charge and b) discharge of symmetric cell test.

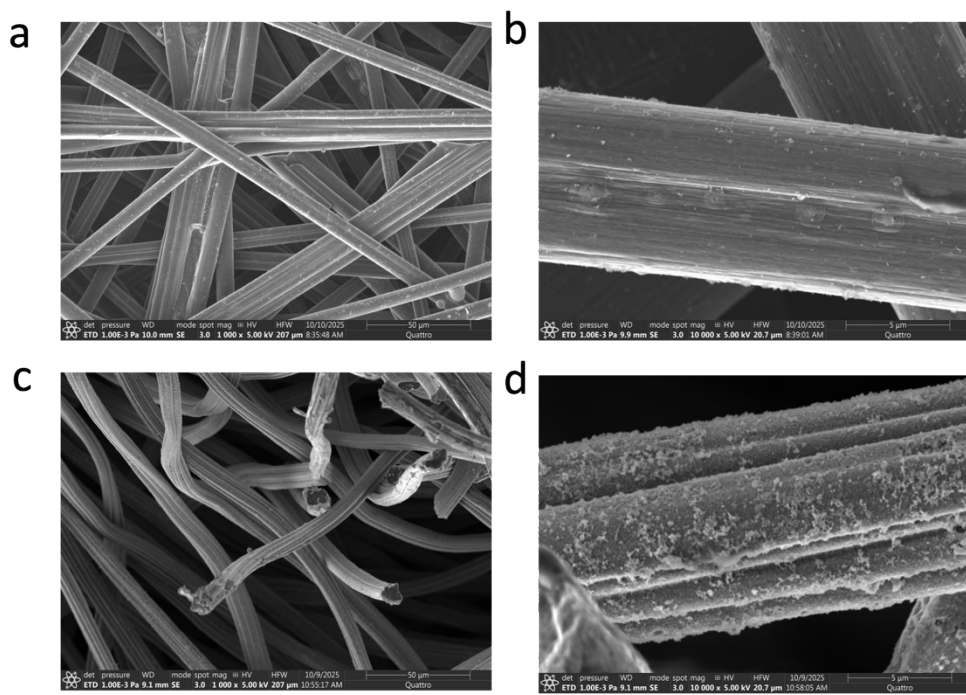


46

47 **Figure S4.** Charge-discharge curve of CP and CF working as electrodes for Ce side. a) 10 mins,
48 b) 30 mins, c) 60 mins.

49

50

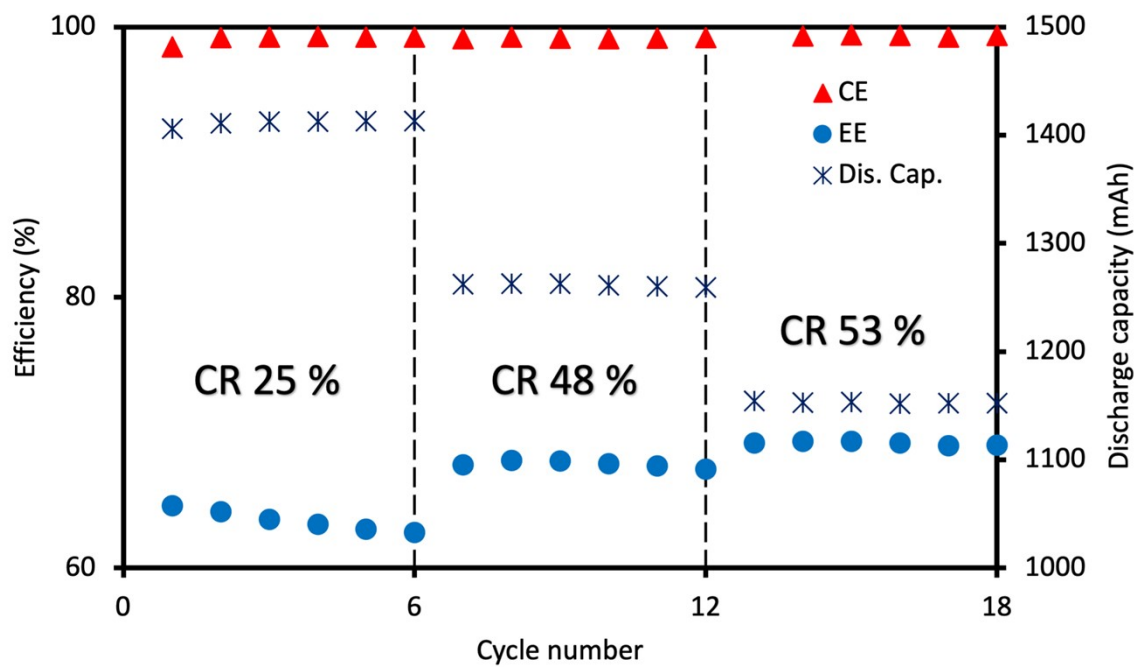


51

52 **Figure S5.** SEM of CP (a and b) and CF (c and d) after being used as Ce side electrode for Ti-Ce
53 RFB test.

54

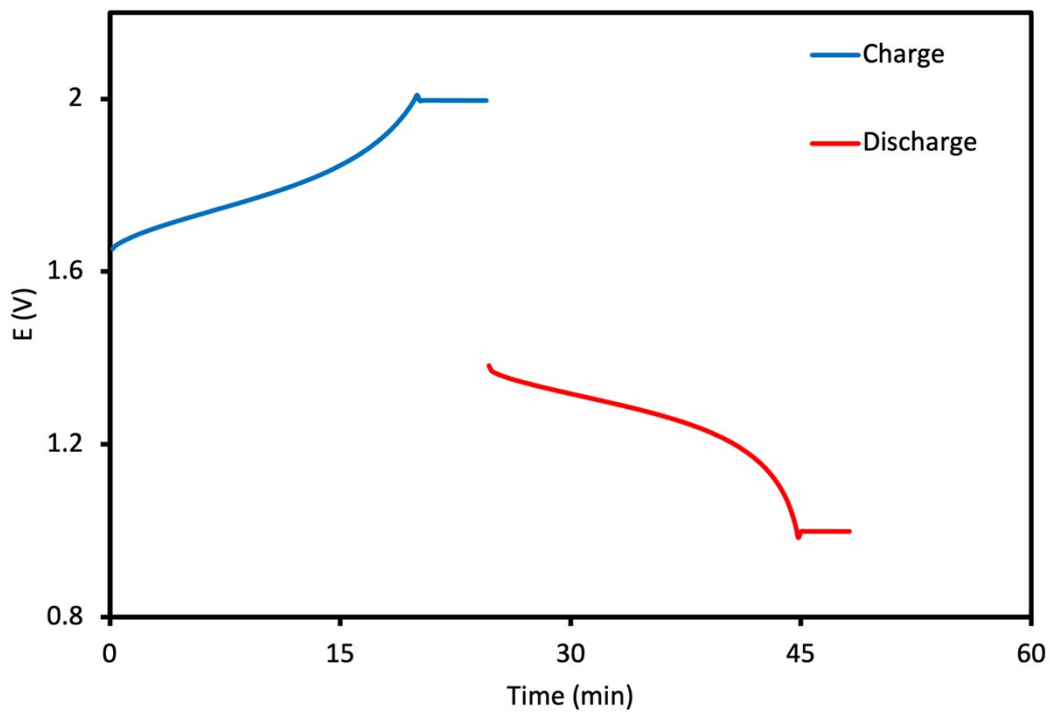
55



56

57 **Figure S6.** Ti-Ce RFB performance with different compression ratios (CR) for Ti side electrode.
58 (Galvanostatic 150 mA cm⁻² plus potentiostatic at 2/1 V for charge/discharge).

59



60

61 **Figure S7.** Charge-discharge curve of optimized RFB cell with CP/HT CF as the electrode of
62 Ce/Ti side with galvanostatic 150 mA cm^{-2} plus potentiostatic at 2/1 V for charge/discharge.

63

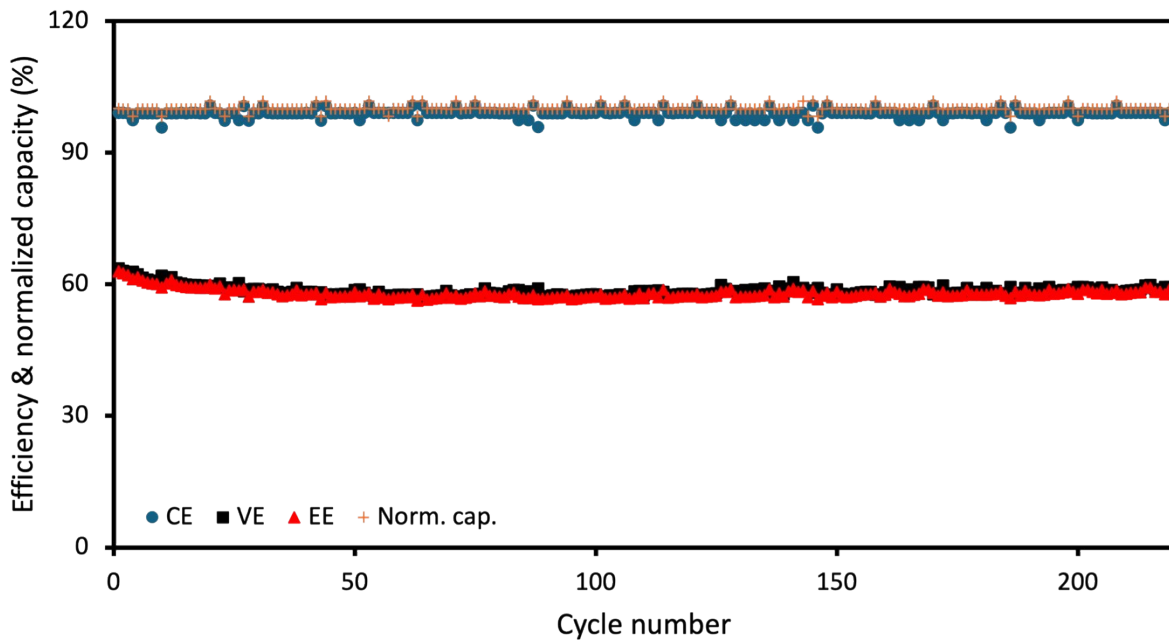
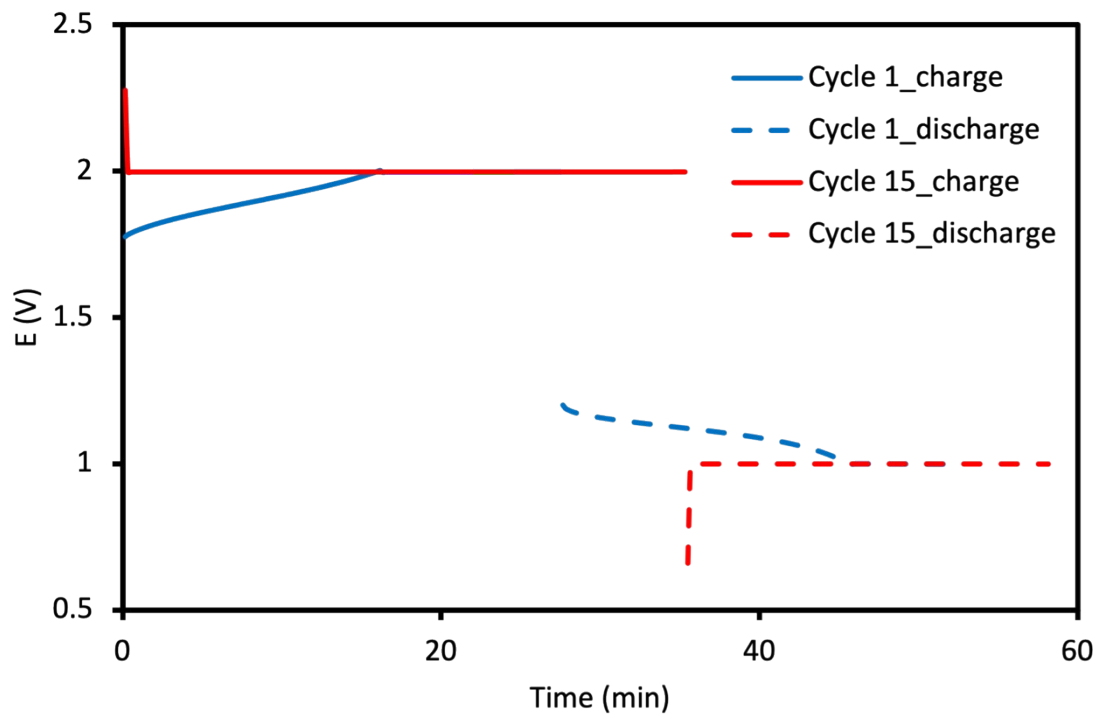


Figure S8. Long-term cycling performance of optimized RFB cell with CP/HT CF as the electrode of Ce/Ti side with galvanostatic charge & discharge at 150 mA cm^{-2} between an operation window of 2 V to 0.5 V and 10-min cutoff for both charge & discharge.

64

65 **Figure S8.** Long-term cycling performance of optimized RFB cell with CP/HT CF as the
66 electrode of Ce/Ti side with galvanostatic charge & discharge at 150 mA cm^{-2} between an
67 operation window of 2 V to 0.5 V and 10-min cutoff for both charge & discharge.

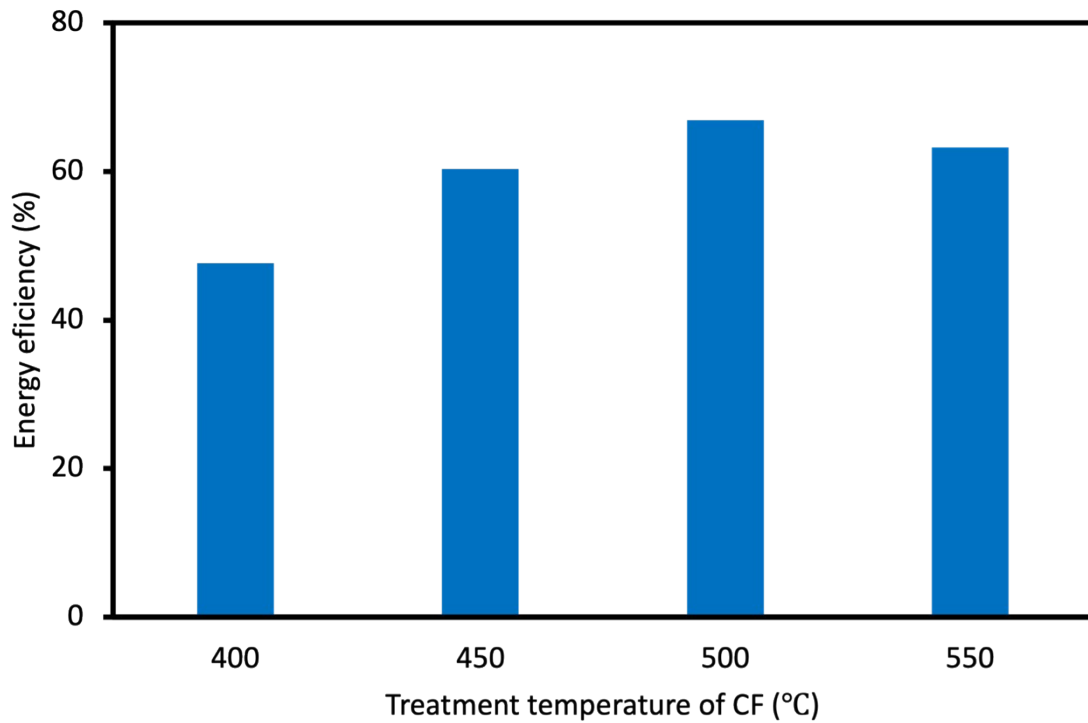
68



69

70 **Figure S9.** Charge-discharge curve of first and last cycle of CF as Ce side electrode in Figure 6b.

71



72

73

Figure S10. Carbon felt pretreatment temperature optimization.

74

75

Table S1. Properties of carbon paper (CP) and carbon felt (CF)

Carbon electrode	Thickness (mm)	Bulk density (g/cm ³)	Porosity (%)	Electrical resistivity (through plane) (mΩ cm)	Flexural strength (MPa)	Flexural modulus (GPa)
CP	0.19	0.44	78	75	45	15
CF	6	0.08	95	< 1200	*	*

77 * Not provided by vendor.

79

Table S2. C_s of CP and CF with 1 cm² geometrical surface area

Electrodes	C_s (mF/cm ²)
CP	0.0773
HT CP	0.0253
CF	0.00772
HT CF	363.4

80

81

Table S3. Atomic ratios (%) of different elements from EDX

Elements	CP before cycling	CP after cycling	CF before cycling	CF after cycling
C	99.6	98.0	99.9	75.9
O	0.4	1.2	0.1	15.6
S	0	0.1	0	5.7
Ce	0	0.7	0	2.8

82

83

84

85 Reference

86 [1] Y. Xie, and Y. Zhou. "Enhanced Capacitive Performance of Activated Carbon Paper Electrode
87 Material." *Journal of Materials Research* 34, no. 14 (2019): 2472–81.
88 <https://doi.org/10.1557/jmr.2019.224>.

89

90 [2] G. Lou, Y. Wu, X. Zhu, et al. "Facile Activation of Commercial Carbon Felt as a Low-Cost Free-
91 Standing Electrode for Flexible Supercapacitors." *ACS Applied Materials & Interfaces* 10, no. 49 (2018):
92 42503–12. <https://doi.org/10.1021/acsami.8b16881>.

93

94 [3] P.C. Ghimire, A. Bhattarai, R. Schweiss, G.G. Scherer, N. Wai, and Q. Yan, "A Comprehensive Study
95 of Electrode Compression Effects in All Vanadium Redox Flow Batteries Including Locally Resolved
96 Measurements." *Applied Energy* 230 (November 2018): 974–82.
97 <https://doi.org/10.1016/j.apenergy.2018.09.049>

98

99 [4] J. Charvát, P. Mazúr, J. Dundálek, et al., "Performance Enhancement of Vanadium Redox Flow Battery
100 by Optimized Electrode Compression and Operational Conditions." *Journal of Energy Storage* 30 (August
101 2020): 101468. <https://doi.org/10.1016/j.est.2020.101468>

102

103 [5] R. Gundlapalli, and S. Jayanti, "Effect of Electrode Compression and Operating Parameters on the
104 Performance of Large Vanadium Redox Flow Battery Cells." *Journal of Power Sources* 427 (July 2019):
105 231–42. <https://doi.org/10.1016/j.jpowsour.2019.04.059>

106

107 [6] W.H. Wang, and X.D. Wang, "Investigation of Ir-Modified Carbon Felt as the Positive Electrode of an
108 All-Vanadium Redox Flow Battery." *Electrochimica Acta* 52, no. 24 (August 2007): 6755–62.
109 <https://doi.org/10.1016/j.electacta.2007.04.121>

110

111 [7] Z. He, Y. Jiang, Y. Li, et al., "Carbon Layer-Exfoliated, Wettability-Enhanced, SO₃H-Functionalized
112 Carbon Paper: A Superior Positive Electrode for Vanadium Redox Flow Battery." *Carbon* 127 (February
113 2018): 297–304. <https://doi.org/10.1016/j.carbon.2017.11.006>